Preprints of the 21st IFAC World Congress (Virtual)
Berlin, Germany, July 12-17, 2020

Dual Quaternion Delay Compensating Maneuver Regulation for Fully Actuated UAVs

Giulia Michieletto * **Nicola Lissandrini** * **Andrea Antonello** *
Riccardo Antonello * **Angelo Cenedese** *

* *Dept. of Information Engineering, University of Padova, Italy*
(corresponding author e-mail: giulia.michieletto@unipd.it)

Abstract: In aerial robotics, path following constitutes a popular task requiring a vehicle to pursue a given trajectory. Resting upon the fulfillment of a desired time law, trajectory tracking techniques often turn out to be ineffective in presence of external disturbances, favoring the adoption of maneuver regulation strategies wherein the desired trajectory is parameterized in terms of the path-variable. In this scenario, this work proposes a new delay-compensating maneuver regulation controller for fully actuated aerial vehicles, whose aim is to guarantee the perfect tracking of a given path in the shortest time interval. The innovative aspect of such a solution relies on the introduction of a recovery term that compensates for possible delays in the task execution. The dual-quaternion formalism is adopted to model the dynamics of the aerial platforms allowing feedback linearization of the whole system, including both position and attitude, with a single controller. The tests conducted in Gazebo physics simulator show that the proposed controller outperforms the popular trajectory tracking PID regulators.

Keywords: autonomous vehicles, path control, feedback linearization, dual quaternions

1. INTRODUCTION

Thanks to their high versatility and maneuverability, nowadays Unmanned Aerial Vehicles (UAVs) have become a mature technology for a wide range of applications in civil, military and industrial contexts (Valavanis and Vachtsevanos, 2015). In most of these ones the platforms are required to accomplish a *path following* task, i.e., to fly along a given trajectory. The most popular path following solutions consist in either linear or nonlinear *trajectory tracking* controllers that force the given vehicle to follow a timed reference state (see, e.g., (Lee and Kim, 2017) and the references therein). Since at each time instant the UAV is required to minimize the error between its actual state and the desired one, the performance of the majority of these solutions degrade in presence of external disturbances as, e.g., unknown wind patterns, air flows due to exogenous sources or other vehicles/objects proximity effects. An unexpected disturbance could unpredictably modify the UAV dynamics, causing, for example, the actuators saturation or an abrupt deviation from the desired path. To overcome these drawbacks, *maneuver regulation* approach can be exploited. This aims at reducing the distance between the current state and the entire desired path, i.e., at following a geometric reference profile without a predefined time scheduling (Spedicato et al., 2016a,b).

In (Hauser and Hindman, 1995) it is proved that for feedback linearizable systems a (stable) maneuver regulation control law can be derived from a stable trajectory tracking control law. Inspired by these results, several authors have compared the performance of these two path following approaches by accounting for different systems and control tasks. For instance, in (Al-Hiddabi and McClamroch, 2002) attention is focused on the hovering control of a vertical takeoff and landing (VTOL) aerial vehicle, while in (Spedicato et al., 2016b) experimental tests are conducted on a VTOL quadrotor required to pursuit a planar circular path. In both cases, the maneuver regulation controller causes the VTOL platform to converge to the desired path in a smooth way with much smaller transient errors than for the trajectory tracking controller.

Along the same research line, our previous paper (Antonello et al., 2018) copes with the maneuver regulation for generic rigid bodies acting in 3D space, in contrast with traditional trajectory tracking solutions. The present work aims at extending the achieved results in two directions: (*i*) focusing on the class of fully-actuated aerial vehicles and (*ii*) accounting for the possible delays emerging in the path following task execution. In detail, by adopting the dual quaternion formalism, a dynamic model is initially provided for multi-rotor platforms having an arbitrary number of propellers, spinning around generically tilted axes (Michieletto et al., 2017). Then, similarly to (Antonello et al., 2018), the derived equations of motion are linearized through the input/output feedback linearization method, allowing the design of a maneuver regulation controller that, using the dual quaternion convention, seeks at stabilizing both the attitude and position of the given UAV. Note that control strategies based on dual quaternion pose representation are not very popular, however this approach provides a unified solution for the attitude and position tracking problem in 3D space (Filipe and Tsiotras, 2013). Finally, the designed maneuver controller is enriched through the introduction of a recovery term

⋆ Part of this work was supported by MIUR (Italian Minister for Education) under the initiative "Departments of Excellence".

that accounts for delay emergence allowing the path following task execution in the shortest time interval. The validity of the proposed delay-compensating maneuver regulation controller is confirmed by the results of the simulation campaign conducted in realistic virtual environment based on a real-time physics engine.

The rest of the paper is organized as follows. Sec. 2 summarizes the principal aspects of the dual quaternion algebra. In Sec. 3 the linearized model for the dynamics of fully-actuated multi-rotors is derived. Sec. 4 describes our dual-quaternion delay-compensating maneuver regulation controller, whose performance are discussed in Sec. 5 through simulative results. Sec. 6 recaps the main conclusions.

2. MATHEMATICAL PRELIMINARIES

A (single) *quaternion* $\mathbf{q}$, belonging to the *quaternion set* $\mathbb{Q}$, constitutes an extension of a complex number to $\mathbb{R}^4$. Formally, this is defined as

$$\mathbf{q} = q_0 + q_1 i + q_2 j + q_3 k \tag{1}$$

with $i^2 = j^2 = k^2 = ijk = -1$ and $q_0, q_1, q_2, q_3 \in \mathbb{R}$. Hereafter the more convenient vector-based representation $\mathbf{q} = [q_0 \;\; \bar{\mathbf{q}}]^\top$ is used, where $q_0 \in \mathbb{R}$ and $\bar{\mathbf{q}} = [q_1 \; q_2 \; q_3] \in \mathbb{R}^3$ identify the *scalar* and the *vector part* of $\mathbf{q}$, respectively.

Being $\bar{\mathbf{0}} = [0\,0\,0] \in \mathbb{R}^3$, $\mathbf{q}_I = \begin{bmatrix}1 & \bar{\mathbf{0}}\end{bmatrix}^\top, \mathbf{q}_N = \begin{bmatrix}0 & \bar{\mathbf{0}}\end{bmatrix}^\top \in \mathbb{Q}$ indicate the *identity* and *null* quaternions, respectively. In addition, given $\mathbf{p}, \mathbf{q} \in \mathbb{Q}$, the principal operations in the quaternion algebra are the following:

$$\text{conjugation} \qquad \mathbf{q}^* = [q_0 \;\; -\bar{\mathbf{q}}]^\top, \tag{2}$$

$$\text{cross product} \qquad \mathbf{p} \times \mathbf{q} = [0 \;\; p_0\bar{\mathbf{q}} + q_0\bar{\mathbf{p}} + \bar{\mathbf{p}} \times \bar{\mathbf{q}}]^\top, \tag{3}$$

$$\text{multiplication} \qquad \mathbf{p} \otimes \mathbf{q} = [p_0 q_0 - \bar{\mathbf{p}} \cdot \bar{\mathbf{q}} \;\; p_0\bar{\mathbf{q}} + q_0\bar{\mathbf{p}} + \bar{\mathbf{p}} \times \bar{\mathbf{q}}]^\top. \tag{4}$$

When $\|\mathbf{q}\|^2 = q_0^2 + \bar{\mathbf{q}} \cdot \bar{\mathbf{q}} = 1$, i.e., the quaternion $\mathbf{q}$ belongs to the hypersphere $\mathbb{Q}_u$ embedded in $\mathbb{R}^4$, this is called *unit quaternion* and can be used to describe a rotation in 3D space. In detail, accounting for two coordinates system $\mathscr{F}_X$ and $\mathscr{F}_Y$ such that $\mathscr{F}_X$ is rotated of an angle $\theta \in (-\pi, \pi]$ about a unit vector $\bar{\mathbf{n}} \in \mathbb{R}^3$ w.r.t. $\mathscr{F}_Y$, their relative orientation can be represented by the unit quaternion

$$\mathbf{q}_{XY} = \begin{bmatrix}\cos\frac{\theta}{2} & \sin\frac{\theta}{2}\bar{\mathbf{n}}\end{bmatrix}^\top \in \mathbb{Q}_u. \tag{5}$$

A *dual quaternion* $\hat{\mathbf{q}} \in \mathbb{D}$, with $\mathbb{D}$ denoting the *dual quaternion set*, represents a generalization of a dual number. Introducing the *nilpotent dual unit* ϵ so that $\epsilon^2 = 0$, $\epsilon \neq 0$, this is indeed defined as

$$\hat{\mathbf{q}} = \mathbf{q}_r + \epsilon \mathbf{q}_d, \tag{6}$$

where the (single) quaternions $\mathbf{q}_r, \mathbf{q}_d \in \mathbb{Q}$ denote the *real* and *dual* part of $\hat{\mathbf{q}}$, respectively.

Similarly to the quaternions case, a dual quaternion $\hat{\mathbf{q}}$ is called *unit dual quaternion* if $\|\hat{\mathbf{q}}\| = \hat{\mathbf{q}}^* \otimes \hat{\mathbf{q}} = \mathbf{q}_I + \epsilon\mathbf{q}_N$, where $\hat{\mathbf{q}}^* = \mathbf{q}_r^* + \epsilon\mathbf{q}_d^*$ is the conjugate of $\hat{\mathbf{q}}$ and the symbol $\otimes$ indicates the multiplication operation in $\mathbb{D}$, defined as follows for two generic dual quaternions $\hat{\mathbf{p}}, \hat{\mathbf{q}} \in \mathbb{D}$

$$\hat{\mathbf{p}} \otimes \hat{\mathbf{q}} = \mathbf{p}_r \otimes \mathbf{q}_r + \epsilon(\mathbf{p}_r \otimes \mathbf{q}_d + \mathbf{p}_d \otimes \mathbf{q}_r). \tag{7}$$

A unit dual quaternion belongs to the unit dual quaternion set $\mathbb{D}_u$ and can be used to describe both rotation and translation in 3D space. Indeed, given two coordinates systems $\mathscr{F}_X$ and $\mathscr{F}_Y$, their relative roto-translation can be expressed through $\hat{\mathbf{q}}_{XY} \in \mathbb{D}_u$: this dual quaternion derives from the combination of the unit (single) quaternion $\mathbf{q}_{XY} \in \mathbb{Q}_u$, representing the relative orientation between the two coordinates systems, and the vector $\mathbf{p}_Y = [0 \;\; \bar{\mathbf{p}}_Y]^\top \in \mathbb{R}^4$, with $\bar{\mathbf{p}}_Y \in \mathbb{R}^3$, indicating the position of the origin of $\mathscr{F}_X$ in $\mathscr{F}_Y$. Formally, it holds that

$$\hat{\mathbf{q}}_{XY} = \mathbf{q}_{XY} + \frac{\epsilon}{2}\mathbf{p}_Y \otimes \mathbf{q}_{XY}. \tag{8}$$

The time derivative of the dual quaternion in (8) is then given by the differential equation

$$\dot{\hat{\mathbf{q}}}_{XY} = \frac{1}{2}\,\hat{\mathbf{q}}_{XY} \otimes \hat{\boldsymbol{\omega}}_X, \tag{9}$$

where $\hat{\boldsymbol{\omega}}_X$ is the so-called *dual velocity*, expressed in $\mathscr{F}_X$. This is the combination of the linear and angular velocities. Specifically, let $\boldsymbol{\omega}_X = [0 \;\; \bar{\boldsymbol{\omega}}_X]^\top, \mathbf{v}_X = [0 \;\; \bar{\mathbf{v}}_X]^\top \in \mathbb{R}^4$ be such that $\bar{\boldsymbol{\omega}}_X, \bar{\mathbf{v}}_X \in \mathbb{R}^3$ are the angular velocity of $\mathscr{F}_X$ w.r.t. $\mathscr{F}_Y$ and the linear velocity of the origin of $\mathscr{F}_X$, respectively, both expressed in $\mathscr{F}_X$. Then, it follows that

$$\hat{\boldsymbol{\omega}}_X = \boldsymbol{\omega}_X + \epsilon\mathbf{v}_X. \tag{10}$$

To conclude, note that all the dual quantities can be represented as eight-dimensional vectors, e.g., $\hat{\mathbf{q}} = [q_{r,0} \; \bar{\mathbf{q}}_r \;\; q_{d,0} \; \bar{\mathbf{q}}_d]^\top$, where $q_{r,0}, q_{d,0} \in \mathbb{R}$ and $\bar{\mathbf{q}}_r, \bar{\mathbf{q}}_d \in \mathbb{R}^3$.

3. DUAL QUATERNION MULTI-ROTOR MODEL

In this section, a linearized dynamic model is provided for the class of generically tilted multi-rotor UAVs introduced in (Michieletto et al., 2017), adopting the dual quaternions formalism to represent the vehicle state. A platform in this class is a UAV whose dynamics depends on $n \geq 4$ lightweight propellers spinning around rotation axes that could be generically oriented. Generally speaking, a given aerial vehicle could be either an under-actuated or a fully actuated system (Ryll et al., 2016), according to the number n of rotors and the mutual orientation of their spinning axes. In the rest of the paper, the analysis is focused on multi-rotor platforms with six controllable degrees of freedom, i.e., on fully actuated UAVs.

3.1 Kinematic and Dynamic Equations

To describe the kinematics and dynamics of the aforementioned aerial vehicles, two coordinates systems are introduced: the global *world frame* $\mathscr{F}_W$ and the local *body frame* $\mathscr{F}_B$ attached to the platform so that its origin O_B coincides with the UAV center of mass (CoM). The state of a multi-rotor UAV is thus defined in term of position and attitude through the unit dual quaternion $\hat{\mathbf{q}}_{BW} \in \mathbb{D}_u$, that specifies both the position $\bar{\mathbf{p}}_W \in \mathbb{R}^3$ of O_B in $\mathscr{F}_W$ and the orientation $\mathbf{q}_{BW} \in \mathbb{Q}_u$ of $\mathscr{F}_B$ w.r.t. $\mathscr{F}_W$.

According to (9), the kinematics of the UAV is driven by

$$\dot{\hat{\mathbf{q}}}_{BW} = \frac{1}{2}\,\hat{\mathbf{q}}_{BW} \otimes \hat{\boldsymbol{\omega}}_B, \tag{11}$$

being $\hat{\boldsymbol{\omega}}_B$ the dual velocity introduced in (10), namely

$$\hat{\boldsymbol{\omega}}_B = \boldsymbol{\omega}_B + \epsilon\,\mathbf{v}_B, \tag{12}$$

with $\boldsymbol{\omega}_B = [0 \;\; \bar{\boldsymbol{\omega}}_B]^\top$, $\mathbf{v}_B = [0 \;\; \bar{\mathbf{v}}_B]^\top \in \mathbb{R}^4$, where $\bar{\boldsymbol{\omega}}_B, \bar{\mathbf{v}}_B \in \mathbb{R}^3$ respectively denote the angular velocity of $\mathscr{F}_B$ w.r.t. $\mathscr{F}_W$ and the linear velocity of O_B in $\mathscr{F}_W$, both expressed in the local frame $\mathscr{F}_B$.

The dynamics of the vehicle can be derived using the standard Newton-Euler approach by considering the actuation effect of the propellers. While rotating, each propeller, whose CoM is at $\bar{\mathbf{p}}_i \in \mathbb{R}^3$ in $\mathscr{F}_B$, exerts a *thrust force* $\bar{\mathbf{f}}_i \in \mathbb{R}^3$ and a *drag moment* $\bar{\boldsymbol{\tau}}_i \in \mathbb{R}^3$, both applied at $\bar{\mathbf{p}}_i$ and oriented along the direction defined by its spinning axis. The overall effect of the set of actuators (expressed in the body frame), results in the *total control force* $\bar{\mathbf{f}}_B^c = \sum_i \bar{\mathbf{f}}_i \in \mathbb{R}^3$ and the *total control torque* $\bar{\boldsymbol{\tau}}_B^c = \sum_i (\bar{\mathbf{p}}_i \times \bar{\mathbf{f}}_i + \bar{\boldsymbol{\tau}}_i) \in \mathbb{R}^3$, both acting at the platform CoM. In particular, for fully actuated platforms the total control force and the total control torque can be independently assigned in a subset of $\mathbb{R}^3$ containing the origin. This is for instance the case of tilted hexarotor described in (Ryll et al., 2019).

By introducing, then, the *dual force* $\hat{\mathbf{f}}_B^c = \mathbf{f}_B^c + \epsilon \boldsymbol{\tau}_B$, with $\mathbf{f}_B^c = \begin{bmatrix} 0 & \bar{\mathbf{f}}_B^c \end{bmatrix}^\top$, $\boldsymbol{\tau}_B^c = \begin{bmatrix} 0 & \bar{\boldsymbol{\tau}}_B^c \end{bmatrix}^\top \in \mathbb{R}^4$, and by adopting the vector notation introduced at the end of Sec. 2 for dual quantities, the dynamics of a given multi-rotor UAV is

$$(\dot{\hat{\boldsymbol{\omega}}}_B)^{\mathsf{S}} = \mathbf{M}^{-1}(\hat{\mathbf{f}}_B^c + \hat{\mathbf{f}}_B^g - \hat{\boldsymbol{\omega}}_B \times \mathbf{M} \cdot (\hat{\boldsymbol{\omega}}_B)^{\mathsf{S}}), \tag{13}$$

where the (dual quaternion) swap operation $(\cdot)^{\mathsf{S}}$ is defined so that $\hat{\mathbf{q}}^{\mathsf{S}} = (\mathbf{q}_r + \epsilon \mathbf{q}_d)^{\mathsf{S}} = \mathbf{q}_d + \epsilon \mathbf{q}_r$ and the term $\hat{\mathbf{f}}_B^g = \mathbf{f}_B^g + \epsilon \mathbf{q}_N$, with $\mathbf{f}_B^g = \mathbf{q}_{BW}^{-1} \otimes [0\ 0\ 0\ -mg]^\top \otimes \mathbf{q}_{BW} \in \mathbb{R}^4$ accounts for the gravity action. The *dual inertia matrix* proposed in (Filipe and Tsiotras, 2013) is used in (13): this is

$$\mathbf{M} = \begin{bmatrix} 1 & \mathbf{0}_{1\times 3} & \mathbf{0}_{4\times 4} \\ \mathbf{0}_{3\times 1} & m\,\mathbf{I}_{3\times 3} & \\ \hline \mathbf{0}_{4\times 4} & & \begin{matrix} 1 & \mathbf{0}_{1\times 3} \\ \mathbf{0}_{3\times 1} & \mathbf{J}_B \end{matrix} \end{bmatrix} \in \mathbb{R}^{8\times 8}, \tag{14}$$

where $\mathbf{I}_{3\times 3}$ indicates the three-dimensional identity matrix, $\mathbf{0}_{i\times j}$ represents a $(i \times j)$ zero matrix, $m \in \mathbb{R}^+$ is the mass of the platform and $\mathbf{J}_B \in \mathbb{R}^{3\times 3}$ is its inertia matrix computed about its center of mass and expressed in $\mathscr{F}_B$. Under the hypothesis of perfect balancing and a suitable choice for $\mathscr{F}_B$, $\mathbf{J}_B$ is assumed to be a diagonal matrix whose non-zero entries are $J_1, J_2, J_3 \in \mathbb{R}^+$.

3.2 Dynamics Linearization

The derived dynamic model (13) can be linearized through the standard *input-output state feedback linearization* method proceeding as in (Antonello et al., 2018). Note that differently from our previous work, the gravity action is considered in (13). In the following it will show that it is possible to dropping out the term $\hat{\mathbf{f}}_B^g$ and considering the system introduced in (Antonello et al., 2018), i.e.,

$$(\dot{\hat{\boldsymbol{\omega}}}_B)^{\mathsf{S}} = \mathbf{M}^{-1}(\hat{\mathbf{f}}_B^c - \hat{\boldsymbol{\omega}}_B \times \mathbf{M} \cdot (\hat{\boldsymbol{\omega}}_B)^{\mathsf{S}}), \tag{15}$$

and then proving that the derived control input linearizes the original system (13) through to the introduction of an additional feedback component (Lemma 1).

According to (Antonello et al., 2018), system (15) can be rewritten in state-space form defining the *state, input and output vectors* as follows

$$\mathbf{x} = \begin{bmatrix} \hat{\mathbf{q}}_{BW} & \bar{\boldsymbol{\omega}}_B & \bar{\mathbf{v}}_B \end{bmatrix}^\top \in \mathbb{R}^{14}, \tag{16}$$

$$\mathbf{u} = \begin{bmatrix} \bar{\boldsymbol{\tau}}_B & \bar{\mathbf{f}}_B \end{bmatrix}^\top \in \mathbb{R}^6, \tag{17}$$

$$\mathbf{y} = \begin{bmatrix} \bar{\mathbf{q}}_r & \bar{\mathbf{q}}_d \end{bmatrix}^\top \in \mathbb{R}^6. \tag{18}$$

The output accounts only for the vector components of the real and dual part of $\hat{\mathbf{q}}_{BW}$ (represented as an eight-dimensional row vector in (16)), since the scalar components $q_{r,0}$, $q_{d,0}$ can be retrieved through the unit norm property. Moreover, because of the fully actuation assumption, the input coincides with the vector components of both the total control force and total control torque. The choice (16)-(18) allows to identify the maps $f(\mathbf{x}) \in \mathbb{R}^{14}$, $g(\mathbf{x}) \in \mathbb{R}^{14\times 6}$ and $h(\mathbf{x}) \in \mathbb{R}^6$ that are needed to rewrite the system (15) as follows

$$\dot{\mathbf{x}} = f(\mathbf{x}) + g(\mathbf{x})\mathbf{u}, \quad \mathbf{y} = h(\mathbf{x}), \tag{19}$$

and then to determine the feedback-linearizing control input $\mathbf{u}$ in terms of the *new input* $\boldsymbol{\mu} \in \mathbb{R}^6$ as

$$\mathbf{u} = -\mathbf{E}^{-1}(\mathbf{x})\mathbf{D}(\mathbf{x}) + \mathbf{E}^{-1}(\mathbf{x})\boldsymbol{\mu}, \tag{20}$$

where the expression of $\mathbf{E}(\mathbf{x}) \in \mathbb{R}^{6\times 6}$ and $\mathbf{D}(\mathbf{x}) \in \mathbb{R}^6$ is the same provided in (Antonello et al., 2018). Considering then the change of coordinates given by $T(\mathbf{x}) = \begin{bmatrix} \mathbf{w}^\top & \mathbf{z}^\top \end{bmatrix}^\top \in \mathbb{R}^{14}$, $\mathbf{w} = \begin{bmatrix} q_{r,0} & q_{d,0} \end{bmatrix}^\top \in \mathbb{R}^2$, $\mathbf{z} = \begin{bmatrix} \bar{\mathbf{q}}_r & \bar{\mathbf{q}}_d & \dot{\bar{\mathbf{q}}}_r & \dot{\bar{\mathbf{q}}}_d \end{bmatrix}^\top \in \mathbb{R}^{12}$ with $\dot{\bar{\mathbf{q}}}_r = [\dot{q}_{r,1}\ \dot{q}_{r,2}\ \dot{q}_{r,3}]$, $\dot{\bar{\mathbf{q}}}_d = [\dot{q}_{d,1}\ \dot{q}_{d,2}\ \dot{q}_{d,3}]^\top \in \mathbb{R}^3$, the system (19) can be written as

$$\dot{\mathbf{w}} = \varsigma(\mathbf{w}, \mathbf{z}) \tag{21}$$

$$\dot{\mathbf{z}} = \mathbf{A}\mathbf{z} + \mathbf{B}\boldsymbol{\mu}, \tag{22}$$

$$\mathbf{y} = \mathbf{C}\mathbf{z}, \tag{23}$$

where $\varsigma : \mathbb{R}^2 \times \mathbb{R}^{12} \to \mathbb{R}^{12}$ and

$$\mathbf{A} = \begin{bmatrix} \mathbf{0}_{6\times 6} & \mathbf{I}_{6\times 6} \\ \mathbf{0}_{6\times 6} & \mathbf{0}_{6\times 6} \end{bmatrix}, \quad \mathbf{B} = \begin{bmatrix} \mathbf{0}_{6\times 6} \\ \mathbf{I}_{6\times 6} \end{bmatrix}, \quad \mathbf{C} = [\mathbf{I}_{6\times 6}\ \mathbf{0}_{6\times 6}]. \tag{24}$$

Although system (22)-(23) corresponds to the linearized form of (15), the following lemma ensures that the original system (13), accounting for the gravity term $\hat{\mathbf{f}}_B^g(\mathbf{x})$, can be stabilized by introducing an additional feedforward term in the control input (20).

Lemma 1. Let $\mathbf{u}_f(\mathbf{x})$ be the feedback linearizing control law (20) for the system (15). Then the following input vector ensures the linearization of the system (13)

$$\mathbf{u}_g(\mathbf{x}) = \mathbf{u}_f(\mathbf{x}) - [\mathbf{0}_{2\times 1}\ \mathbf{f}_B^g(\mathbf{x})^\top]^\top. \tag{25}$$

Proof. System (19) can be modified in order to account for the gravity force, namely to correspond to the state-space form of system (13). In detail, it results to be

$$\dot{\mathbf{x}} = f(\mathbf{x}) + g(\mathbf{x})\mathbf{u} + f_g(\mathbf{x}) \tag{26}$$

where the additional term $f_g(\mathbf{x}) \in \mathbb{R}^{14}$ embeds the gravity action so that $f_g(\mathbf{x}) = [\mathbf{0}_{10\times 1}\ m^{-1}\mathbf{f}_B^g(\mathbf{x})^\top]^\top$. The choice $\mathbf{u} = \mathbf{u}_g(\mathbf{x})$ in (25) compensates for the term $f_g(\mathbf{x})$ and system (26) reduces to

$$\dot{\mathbf{x}} = f(\mathbf{x}) + g(\mathbf{x})\mathbf{u}_f(\mathbf{x}). \tag{27}$$

Through the variables change (21), this turns out to be linear by the assumption on $\mathbf{u}_f(\mathbf{x})$. □

4. DUAL QUATERNION MANEUVER REGULATION

This section presents a delay-compensating maneuver regulation controller for the UAVs introduced in Sec. 3. First, the linearized form of the dynamic equations, namely system (22)-(23), is taken into account designing an exponentially stable maneuver regulation scheme proceeding as in (Antonello et al., 2018). Then the proposed solution is extended by adding a *recovery term* that allows to cope with delays emergency in path following task execution.

4.1 Maneuver Regulation Control Design

Given a path following task, the trajectory tracking approach consists in designing a control law ensuring that at each time instant the current vehicle state coincides with a desired one. Differently, when the maneuver regulation approach is considered, the vehicle is not required to chase a virtual target, but just to stay on the desired path.

Formally, a *maneuver* is defined as a set of trajectories in the state-control space that are consistent with the system dynamics. Hence, given the system (22)-(23) and considering the manuever $\{\mathbf{z}_d(\tau), \boldsymbol{\mu}_d(\tau)\}$ with $\tau \in \mathbb{R}_0^+$, the maneuver regulation control goal consists in designing a *time mapping function* $\sigma : \mathbb{R}_0^+ \to \mathbb{R}_0^+,\ t \mapsto \tau$, such that the feedback control law $\boldsymbol{\mu} = \beta(\mathbf{z}, \mathbf{z}_d(\sigma(t)), \boldsymbol{\mu}_d(\sigma(t)))$, $\beta\colon \mathbb{R}^{12} \times \mathbb{R}_0^+ \to \mathbb{R}^6$ is exponentially stabilizing. In particular, the function $\sigma(\cdot)$ needs to be defined in order to select the appropriate time warping that, depending on the current vehicle state, minimizes a specified cost (see the approach proposed in (Al-Hiddabi and McClamroch, 2002; Hauser and Hindman, 1995; Spedicato et al., 2016a)).

Given these premises, let introduce the *error vector* $\mathbf{e}(t) = \mathbf{z}(t) - \mathbf{z}_d(\tau^*) \in \mathbb{R}^{12}$, where $\tau^* \in \mathbb{R}_0^+$ is the time to be used in the maneuver regulation, which depends on the current state. A good choice is to select $\tau^* = \sigma(t) = \gamma(\mathbf{z}(t))$ so that $\gamma : \mathbb{R}^{12} \to \mathbb{R}_0^+$ minimizes the gap between the current state and the entire timespan of the trajectory, according to the norm induced by a suitable positive definite matrix $\mathbf{P} \in \mathbb{R}^{12\times 12}$. Formally,

$$\tau^* = \gamma(\mathbf{z}(t)) = \arg\min_{\tau \in \mathbb{R}_0^+} \|\mathbf{z}(t) - \mathbf{z}_d(\tau)\|^2_{\mathbf{P}}. \tag{28}$$

In particular, the matrix $\mathbf{P}$ in (28) can be selected accounting for the following theorem about the convergence of maneuver regulation architecture.

Theorem 2. ((Hauser and Hindman, 1995)). Given a linear system $\dot{\mathbf{x}}(t) = \mathbf{A}\mathbf{z}(t) + \mathbf{B}\boldsymbol{\mu}(t)$ and a desired state-input trajectory $\{\mathbf{z}_d(\cdot), \boldsymbol{\mu}_d(\cdot)\}$, consider a feedback control law $\boldsymbol{\mu}(t) = \boldsymbol{\mu}_d(t) + \mathbf{K}(\mathbf{z}(t) - \mathbf{z}_d(\tau^*))$ with τ^* computed as in (28) so that the closed-loop error dynamics, namely $\dot{\mathbf{e}}(t) = \mathbf{A}_c\mathbf{e}(t)$ with $\mathbf{e}(t) = \mathbf{z}(t) - \mathbf{z}_d(\tau^*)$ and $\mathbf{A}_c = \mathbf{A} + \mathbf{B}\mathbf{K}$, assures uniform asymptotic tracking. Assume that there exists a constant $c \in \mathbb{R}^+$ such that the function $\gamma(\cdot)$ in (28) is well defined on the time-dependent set $\Gamma = \{\mathbf{z}(t) \mid \|\mathbf{z}(t) - \mathbf{z}_d(\tau^*)\|^2_{\mathbf{P}} < c\}$ by choosing the positive definite matrix $\mathbf{P}$ so that the resulting matrix $-(\mathbf{A}_c^\top\mathbf{P} + \mathbf{P}\mathbf{A}_c)$ is positive definite. Then exponentially stable maneuver regulation is provided by the control law

$$\boldsymbol{\mu}(t) = \boldsymbol{\mu}_d(\gamma(\mathbf{z}(t))) + \mathbf{K}(\mathbf{z}(t) - \mathbf{z}_d(\gamma(\mathbf{z}(t)))). \tag{29}$$

In the light of Thm. 2, given a desired trajectory $\mathbf{z}_d(\cdot)$ for system (22)-(23), to design an exponentially stable maneuver regulation controller it is sufficient to define a gain matrix $\mathbf{K} = [\mathbf{K}_p\ \mathbf{K}_d] \in \mathbb{R}^{6\times 12}$, with $\mathbf{K}_p = \mathrm{diag}(\{k_{p,i}\}) \in \mathbb{R}^{6\times 6}$, $\mathbf{K}_d = \mathrm{diag}(\{k_{d,i}\}) \in \mathbb{R}^{6\times 6}$, selecting the scalar gains $k_{p,i}, k_{d,i},\ i = 1\dots 6$, in order to ensure the stability of the full-state feedback system, governed by $\mathbf{A}_c = \mathbf{A} - \mathbf{B}\mathbf{K} \in \mathbb{R}^{6\times 6}$, with $\mathbf{A}$ and $\mathbf{B}$ as in (24). Hence, recalling (29), the maneuver regulation control law is

$$\boldsymbol{\mu}(t) = \boldsymbol{\mu}(\mathbf{z}(t), \mathbf{z}_d(\tau^*)) = -\mathbf{K}(\mathbf{z}(t) - \mathbf{z}_d(\gamma(\mathbf{z}(t)))), \tag{30}$$

with $\gamma(\cdot)$ as in (28) and $\mathbf{P}$ fulfills the assumption of Thm. 2.

Observation 1. Note that, when the mapping function $\gamma(\cdot)$ is not take into account, the design control law (30) corresponds to the implementation of a (stable) PD trajectory tracking controller for the linear system (22)-(23).

4.2 Recovery Term Extension

A drawback of maneuver regulation approach emerges when the trajectory travel time is set as high-priority control requirement. Implementing the solution proposed in the previous section, indeed, the vehicle is required to track the given path without a time scheduling, hence its dynamics could become very slow, especially in the presence of disturbances. In this case, the accrued delay remains unchanged until the end of the task, even with the actuators being far from the saturation threshold. This behavior is evident, for example, in the plots reported in (Antonello et al., 2018) where the considered vehicle experience a temporary stop. In the following, a solution to this issue is proposed modifying the control law (30) to guarantee the minimization of the accumulated (curvilinear) offset, according with the vehicle actuation limits.

The proposed delay-compensating strategy is based on the introduction of an additional term, hereafter referred to as *recovery term*, to the result of the optimization (28). This is defined as a function $\rho(\cdot)$ of the current vehicle state and the desired vehicle state at τ^* as follows

$$\tau^{rc} = \rho(\mathbf{z}(t), \mathbf{z}_d(\tau^*))(t - \tau^*). \tag{31}$$

The function $\rho(\cdot)$ accounts for the actuation limits, that in case of multi-rotor platforms translate into limitations on the maximum propellers spinning rate imposed by the used motors. In detail, let denote with $\mu_{max} \in \mathbb{R}$ the maximum attainable intensity of control input vector (30) due to actuators saturation limits. In order to guarantee that $\|\boldsymbol{\mu}\|_2 \leq \mu_{max}$ while optimizing the vehicle performance in case of delay, it is suitable to select

$$\rho(\mathbf{z}(t), \mathbf{z}_d(\tau^*)) = k_{rc}|\|\boldsymbol{\mu}(t)(\mathbf{z}(t), \mathbf{z}_d(\tau^*))\|_2 - \mu_{max}| \tag{32}$$

where the *recovery gain* $k_{rc} \in \mathbb{R}$ is a tunable parameter.

In the next section, it will be shown that the introduction of the recovery term (31) ensures the path following task execution in the shortest time interval even in case of a completely temporary stop of the vehicle.

5. SIMULATION RESULTS

This section is devoted to the validation of the delay-compensating maneuver regulation solution introduced in Sec. 4, by presenting the results of a simulation campaign carried out exploiting *Robotic Operating System* (ROS) and *Gazebo multi-robot simulator* to approximate the real-world environment. In particular, the aerial vehicle dynamics is simulated employing the *rotorS* libraries (Furrer et al., 2016), which allow for realistic flight simulations, including propeller dynamics and actuation limits, while the control law is implemented in Simulink and interfaced with ROS through the Robotics Toolbox blocks.

The considered fully actuated multi-rotor vehicle is the hexarotor platform depicted in Fig. 1. This is designed tailoring the AscTech Neo 11 model available from rotorS that introduces the possibility to tilt the propellers, guaranteeing the UAV full actuation (Michieletto et al., 2018).

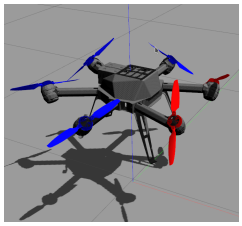

Fig. 1. Fully actuated hexarotor platform.

For this platform, the main control goal consists in a path following task where the vehicle is required to track an outward spiral path, with constant tangential velocity and a given attitude profile. Formally, the desired position trajectory is defined by the function $\alpha\colon [t_0, t_f] \to \mathbb{R}^3$,

$$t \mapsto \begin{cases} x = r(1+\kappa t)\cos(\zeta t + \theta_{\text{in}}) + x_0 \\ y = r(1+\kappa t)\sin(\zeta t + \theta_{\text{in}}) + y_0 \\ z = z_0, \end{cases} \tag{33}$$

where $r \in \mathbb{R}^+$ represents the initial radius of the spiral, $\zeta \in \mathbb{R}$ is the angular velocity, $\theta_{\text{in}} \in (-\pi, \pi]$ is the initial offset angle, $\kappa \in \mathbb{R}^+$ is the spiral rate and $\bar{\mathbf{p}}_0 = [x_0 \;\; y_0 \;\; z_0] \in \mathbb{R}^3$ is the starting point of the curve in the inertial frame $\mathscr{F}_W$. In addition, denoting by (ϕ, θ, ψ) the roll, pitch and yaw angle of the vehicle, a sinusoidal trend is imposed for the rotation both along the x and y-axis.

In detail, the conducted test consists of different phases. At the beginning, the vehicle is required to hover at $\bar{\mathbf{p}}_0$, while being parallel to the ground. Then, at $t_0 = 5$s, the position and attitude trajectory (33) is imposed as reference. To highlight the benefits of the delay-compensating maneuver regulation control strategy, a fictious disturbance is introduced at $t = 9$s. This consists of a complete stop of the vehicle, for a total duration of 7s, mimicking adverse wind gust conditions. When the disturbance is removed, the vehicle is allowed to move and the controller resumed. The disturbance introduction allows to compare the response of three control laws: the PD trajectory tracking method mentioned in Observation 1 for which the control law results to be $\boldsymbol{\mu}(t) = -\mathbf{K}(\mathbf{z}(t) - \mathbf{z}_d(t))$, the maneuver regulation approach (30) (recalled from (Antonello et al., 2018)) and, thirdly, the control law (30) modified through the introduction of the the recovery term (31).

To better appreciate the differences in controllers performance, two metrics are introduced: $\lambda(t) \in \mathbb{R}$, measuring the gap between the actual position $\bar{\mathbf{p}}(t) \in \mathbb{R}^3$ and its projection $\bar{\mathbf{p}}^{\perp}(t) \in \mathbb{R}^3$ on the desired path, and $\Delta(t) \in \mathbb{R}$, consisting in the curvilinear distance along the goal path between the desired position $\bar{\mathbf{p}}_d(t) \in \mathbb{R}^3$ and $\bar{\mathbf{p}}^{\perp}(t)$. Formally, these are given by

$$\lambda(t) = \|\bar{\mathbf{p}}(t) - \bar{\mathbf{p}}^{\perp}(t)\|_2, \tag{34}$$

$$\Delta(t) = \int_{s_1}^{s_2} |\alpha'(\varphi(\bar{\mathbf{p}}))\varphi'(\bar{\mathbf{p}})|\, d\bar{\mathbf{p}}, \tag{35}$$

where $\varphi\colon [\bar{\mathbf{p}}_0 \;\; \bar{\mathbf{p}}_f] \to [t_0 \;\; t_f]$ is a one-to-one and onto map such that $\bar{\mathbf{p}}_0, \bar{\mathbf{p}}_f \in \mathbb{R}^3$ are the starting and final point of the desired trajectory and $s_1 = \varphi(\bar{\mathbf{p}}^{\perp}(t))$ and $s_2 = \varphi(\bar{\mathbf{p}}_d(t))$. In detail, the metric in (34) provides a measure of the capability of the controller to ensure the desired path tracking, whereas (35) allows to quantify the delay accumulated by the controlled vehicle. It is desirable thus to guarantee the lowest possible values for both metrics throughout the whole dynamics.

The results of the simulation are reported in Fig.s 2 and 3. In particular, Fig. 2(a) shows the trajectories of the vehicle in 3D space, for the three different control policies, Fig. 2(b) provides an insight of the controllers performance and Fig. 3 depicts the behavior of the metrics (34)-(35). The time window during which the disturbance is acting is highlighted in gray.

Before the disturbance introduction, the three path following solutions exhibit similar properties, although the adoption of maneuver regulation control law (30) implies the emergence of a slight delay, mainly caused by non idealities in the simulation. The real advantages of the delay-compensating maneuver regulation controller is instead clear after the disturbance action. As expected, the trajectory tracking method allows to zero the accumulated offset (Fig. 3-top). However, this strategy does not necessarily comply with the path following requirements: a spike is observable in Fig. 3-bottom. This could be a potential problem when no-fly zones are introduced in the scenario or when it is mandatory to follow the planned path. On the other hand, the real-time computation of the optimal path following solution is performed through the maneuver regulation approach via law (30). This allows for a full compliance to the path, as can be appreciated in the near-zero behavior of the λ-metric. However, this comes at the price of accumulating a delay confirmed by the increasing trend of Δ-metric in Fig. 3-top. This plot shows also the benefits deriving from the introduction of the recovery term (31) that allows to quickly compensate for the delay caused by the disturbance, similarly to the trajectory tracking solution. Nonetheless, note that this control method ensures also near-zero path following error (Fig. 3-bottom), thus maintaining all the advantages of maneuver regulation approach.

A video of the described path following comparison is available at `https://youtu.be/UD5dayCKrhk`.

6. CONCLUSIONS

Within aerial robotic context, this work copes the path following task for fully actuated multi-rotor platforms whose dynamics is modeled exploiting the Euler-Newton approach by adopting the dual quaternion formalism to describe the vehicle state. The proposed solution follows the maneuver regulation paradigm described in (Antonello et al., 2018) focusing on the compensation of possibly emerging delays. This issue is managed through the introduction of a recovery term in the time optimization that accounts also for the actuation saturation limits. The effectiveness of the designed delay-compensating maneuver regulation control is assessed through a simulative campaign conducted in a virtual environment that approximates the real-world scenario employing a Gazebo-ROS architecture.

REFERENCES

Al-Hiddabi, S.A. and McClamroch, N.H. (2002). Tracking and maneuver regulation control for nonlinear nonminimum phase systems: Application to flight control. *IEEE Trans. on Control Systems Technology*, 10(6), 780–792.

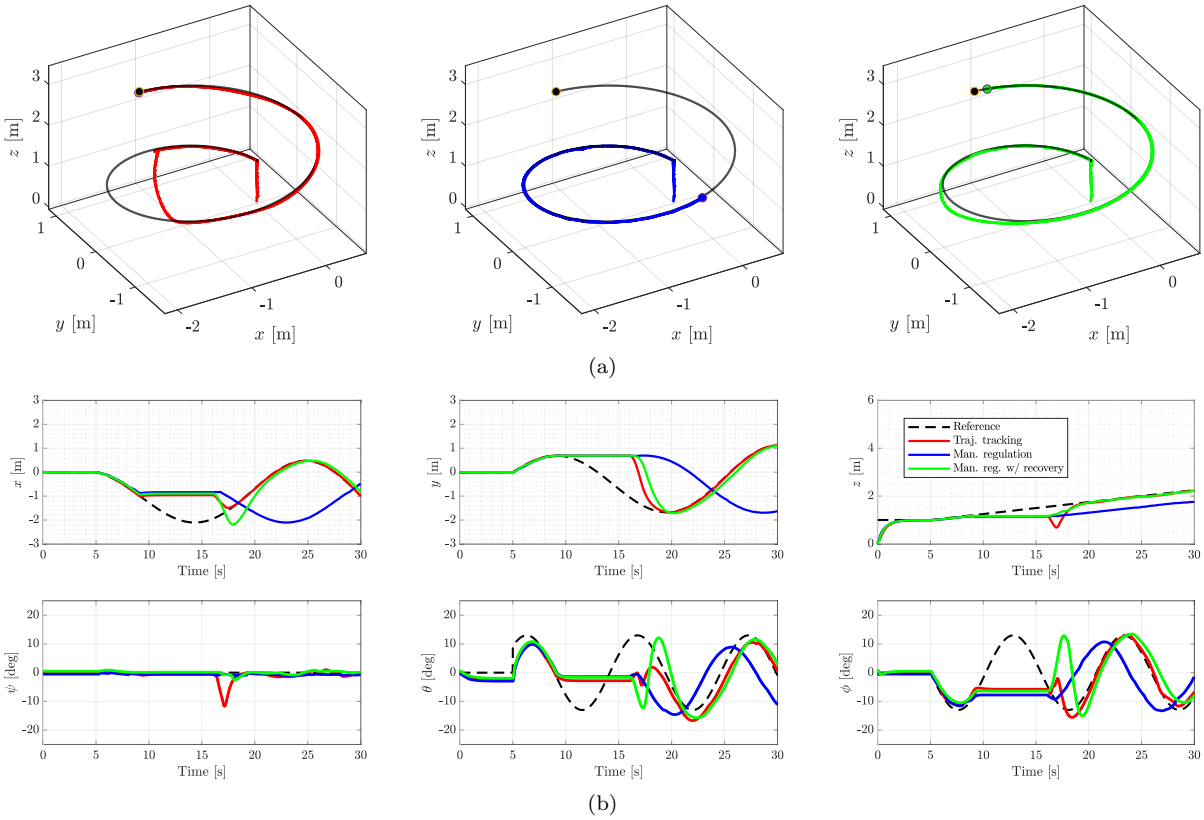

Fig. 2. Comparison of the performance of the analyzed control solutions in position and attitude tracking.

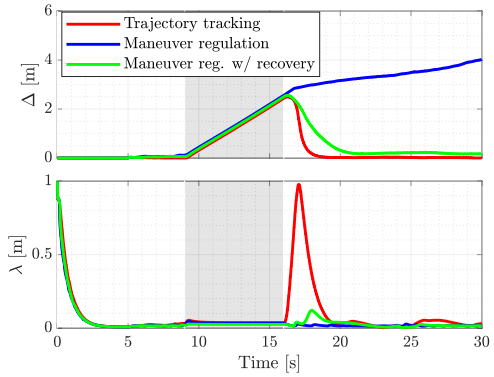

Fig. 3. Performance metrics comparison for the analyzed control solutions.

Antonello, A., Michieletto, G., Antonello, R., and Cenedese, A. (2018). A dual quaternion feedback linearized approach for maneuver regulation of rigid bodies. *IEEE Control Systems Letters*, 2(3), 327–332.

Filipe, N. and Tsiotras, P. (2013). Simultaneous position and attitude control without linear and angular velocity feedback using dual quaternions. In *2013 IEEE American Control Conference*, 4808–4813.

Furrer, F., Burri, M., Achtelik, M., and Siegwart, R. (2016). RotorSA modular gazebo MAV simulator framework. In *Robot Operating System*, 595–625. Springer.

Hauser, J. and Hindman, R. (1995). Maneuver regulation from trajectory tracking: Feedback linearizable systems. *IFAC Proceedings Volumes*, 28(14), 595–600.

Lee, H. and Kim, H.J. (2017). Trajectory tracking control of multirotors from modelling to experiments: A survey. *Int. Jour. of Control, Automation and Systems*, 15(1), 281–292.

Michieletto, G., Ryll, M., and Franchi, A. (2017). Control of statically hoverable multi-rotor aerial vehicles and application to rotor-failure robustness for hexarotors. In *2017 IEEE Int. Conf. on Robotics and Automation,*, 2747–2752.

Michieletto, G., Ryll, M., and Franchi, A. (2018). Fundamental actuation properties of multirotors: Force–moment decoupling and fail–safe robustness. *IEEE Trans. on Robotics*, 34(3), 702–715.

Ryll, M., Bicego, D., and Franchi, A. (2016). Modeling and control of fast-hex: a fully-actuated by synchronized-tilting hexarotor. In *2016 IEEE/RSJ Int. Conf. on Intelligent Robots and Systems*, 1689–1694.

Ryll, M., Muscio, G., Pierri, F., Cataldi, E., Antonelli, G., Caccavale, F., Bicego, D., and Franchi, A. (2019). 6D interaction control with aerial robots: The flying end-effector paradigm. *The Int. Jour. of Robotics Research*, 1045–1062.

Spedicato, S., Franchi, A., and Notarstefano, G. (2016a). From tracking to robust maneuver regulation: An easy-to-design approach for VTOL aerial robots. In *2016 IEEE Int. Conf. on Robotics and Automation*, 2965–2970.

Spedicato, S., Notarstefano, G., Bülthoff, H.H., and Franchi, A. (2016b). Aggressive maneuver regulation of a quadrotor UAV. In *Robotics Research*, 95–112. Springer.

Valavanis, K.P. and Vachtsevanos, G.J. (2015). Uav applications: Introduction. *Handbook of Unmanned Aerial Vehicles*, 2639–2641.